Soft Microtubule Muscle-Driven 3-Axis Skin-Stretch Haptic Devices

MAI THANH THAI, TRUNG THIEN HOANG, PHUOC THIEN PHAN, NIGEL HAMILTON LOVELL, (Fellow, IEEE), AND THANH NHO DO, (Member, IEEE)

Faculty of Engineering, Graduate School of Biomedical Engineering, University of New South Wales, Sydney, NSW 2052, Australia

Corresponding author: Thanh Nho Do (tn.do@unsw.edu.au)

ABSTRACT In the real world, people heavily rely on haptic or touch to manipulate objects. In emerging systems such as assistive devices, remote surgery, self-driving cars and the guidance of human movements, visual or auditory feedback can be slow, unintuitive and increase the cognitive load. Skin stretch devices (SSDs) that apply tangential force to the skin via a tactor can encode a far richer haptic space, not being limited to force, motion, direction, stiffness, indentation and surface geometry. This paper introduces novel hand-worn hydraulic SSDs that can induce 3-axis tangential forces to the skin via a tactor. The developed SSDs are controlled by new soft microtubule muscles (SMMs) which are driven by hydraulic pressure via custom miniature syringes and DC micromotors. An analytical model is developed to characterize the responses of SMM output in terms of force and elongation. A kinematic model for the motion of the 3-axis SSD is also developed. We evaluate the capability of the tactor head to track circular reference trajectories within different working spaces using an optical tracking system. Experimental results show that the developed SSDs have good durability, high-speed, and can generate omnidirectional shear forces and desired displacement up to 1.8 N and 4.5 mm, respectively. The developed SMMs and SSDs created in this paper will enable new forms of haptic communication to augment human performance during daily activities such as tactile textual language, motion guidance and navigational assistance, remote surgical systems, rehabilitation, education, training, entertainment, or virtual and augmented reality.

INDEX TERMS Skin stretch device, haptics, soft muscle, motion guidance, touch display, tactile feedback.

I. INTRODUCTION

The richest form of communication between human beings is achieved via language that is commonly conveyed using visual or auditory modalities. However, visual and auditory cues may be disruptive, and therefore they may be inappropriate in many circumstances [1]. Haptics, or the sense of touch, offers humans the ability to explore the surrounding environment and manipulate objects in daily activities [2]. Haptic stimulation provides an alternative way to convey information, control the balance of amputees, provide motion guidance and navigational assistance, or support surgical training and tactile alphabets [3]. One method for achieving haptic motion guidance is to apply force feedback to the skin via devices that are mechanically grounded through rigid linkages [4]. However, this method requires a large workspace

The associate editor coordinating the review of this manuscript and approving it for publication was Yingxiang Liu.

and bulky and expensive tools. Wearable devices, in contrast, offer compact, flexible, lightweight and low-cost solutions. However, the mechanics of existing wearable devices to interact with human skin still pose many challenges, which severely impacts their usability due to the occlusion of rigid components [5]. In tele-surgical procedures, surgeons benefit from real-time force feedback to prevent excessive force applied to tissues [6]. In medical training, effective haptic devices can be used to enhance the interaction between medical students and clinicians or provide a useful tool to conduct complex training for surgical procedures within virtual organs without accessing real human tissues [7]. Among the many types of haptic devices, vibrotactile displays, which apply vibrations to the skin using vibration motors or linear resonant actuators, are the most widespread and investigated, because of the ease of design and actuation. Several methods to provide directional cues via vibrotactile feedback have been described in the literature [8]. To use vibratory feedback,

users must learn an association between localized vibration cue and a spatial direction which is inherently difficult to localize because cutaneous vibrations spread efficiently across the skin surface, leading to desensitization and sensory adaptation, which can impair device functionality over time. In addition, continuously wearing or touching vibrating devices causes the users' desensitization and discomfort after prolonged use [9]. The effective sensation of vibration feedback can be even decreased when users are in motion. Recently, skin stretch (SS) feedback has been used to guide human motion, render friction or stiffness of the objects or their surface geometry [10]. Several groups have investigated haptic feedback based on tangential force to the skin via a tactor in the form of wearable devices [11], [12]. SS is a known part of the normal physiological apparatus for proprioception, contributing to our sense of motion and location of limbs. The motions and velocities required to impart skin stretch can be slow, allowing the design of compact, low power and portable devices. Skin stretch cues that are perceived by the sensory system via slowly adapting type II (SA-II) stretch sensitive afferent nerve fibers- - -fibers that are widespread in tissues associated with hairy skin deformation- - -have been shown as a promising haptic feedback modality in many applications in the last decade due to several superior features [13]. First, skin stretch devices (SSD) manipulates human skin in a way that is similar to natural haptic interactions. Second, SS feedback can provide 3-D directional cues by combining omnidirectional shear force and one normal force as proven in several studies [14]–[16]. Third, SSDs would be useful in guiding users without distracting visual or auditory sensation [17].

Although several wearable haptic devices have been developed [18], most approaches have focused on wearable tactile feedback devices for the fingertips because the glabrous skin has great density and different types of mechanoreceptors [19]. These haptic devices are able to deliver normal and tangential skin deformation to the finger pad by moving an end effector against the surface of the finger pad while the device itself is grounded to the finger [20], [21]. Despite advances, these devices could not provide effective shear forces to communicate with the skin due to the use of rigid components or low energy efficiency from the actuation systems such as onboard rigid DC motors, piezoelectric actuators, dielectric actuators, or tendon-driven mechanisms. For example, Leonardis *et al.* [22] developed a three-degree of freedom (DoF) skin deformation device that is driven by three rigid servo DC motors through rigid parallel linkages. Although this design shows positive results for grasping objects in virtual environments, it is rigid, bulky and unable to well adapt to the fingertips, which causes discomfort to the users after prolonged use. Solazzi *et al.* [23] designed a portable haptic device to render the interaction force in virtual environments. This device is mounted directly onto the last phalanx of the finger and actuated by bilateral cables via joint pulleys and DC motors located at the forearm. Although this device could perform a simple task of shape exploration, its wearability is still limited by rigid structures,

a heavy weight and large size. Schorr and Okamura [24] fabricated a skin deformation device that can deliver 3-DoF translational skin deformation with a delta parallel mechanism and two rigid DC motors. This design can provide both stiffness and friction discrimination. However, most mechanical and electrical components are bulky and mounted onto a finger, which prevents or restricts the users' movement during operation. Gleeson *et al.* [25] proposed a fingertip-mounted tactile display that could displace and stretch the finger skin in two degrees of freedom via a hemispherical tactor. Any planar motion is simultaneously controlled by two radio control (RC) servo motors and a compliant flexure stage. Nevertheless, it is not a compact wearable device and is heavy. Another interesting device was developed by Minamizawa *et al.* [26]. In this approach, a wearable and ungrounded haptic device could simulate the weight sensations of virtual objects by deforming the fingertip through a DC motor and a belt. However, this design could not render the forces in different directions and needed a single motor for each finger. Recently, soft robotics for SS feedback has been implemented to provide a better interaction with the skin surface. Chossat *et al.* [27] introduced a soft SSD driven by three coiled polymer actuators. Although the design shows promising results in virtual reality, it can only induce a single lateral force and the contraction speed and force amplitude are still low compared to other existing designs. Kanjanapas *et al.* [18] designed a pneumatic 2-DoF soft haptic device that is mounted on the forearm to provide shear force. It consists of four soft fiber-constrained pneumatic actuators attached to a dome-shaped tactor head to generate eight directional forces to the skin surface. Nevertheless, it is bulky due to a large rigid housing and the use of pneumatic source which shows high noise and is bulky because of large fluid transmission tubes. As a result, this device could not adapt to the fingertip and is only employed in large surface areas of skin. In a newer version proposed by Yoshida *et al.* [28], the authors extended the design with a rigid rotational housing that is affixed to a DC motor and three soft fiber-constrained linear pneumatic actuators to enable linear horizontal and vertical movements. This device can simultaneously induce normal and shear forces for haptic vibration and torsional skin deformation cues. However, it was built with a rigid housing and pneumatic actuators, which makes users uncomfortable and desensitized.

Although many studies have concentrated on the mechanoreceptors at the fingertip, there has been less attention to the receptors in non-glabrous skin. Bark *et al.* [6] presented a wearable rotational SSD. They also investigated the pattern of skin motion and strain imparted by the device. This SSD still has rigid components and is not able to provide both normal and omnidirectional shear forces to the skin. In addition, these aforementioned haptic devices are not able to control the threshold of normal and shear forces to the skin areas in ways that are similar to what is felt during human skin-object interaction. During the interaction, the control of force threshold and motion is extremely important because

the way humans sense shear force is highly dependent on their mechanoreceptor density and the distribution of SSDs over the skin surface. Although current SSDs based on soft robotics technology offer high compliance, safety and are lightweight, none of them can effectively induce 3-DoFs skin deformation in the form of finger-worn soft haptic devices. Advances in soft actuation are needed to develop new forms of haptic communication with distributed tactile stimulation in order to promote the progress of science and beneficially impact on human health and life.
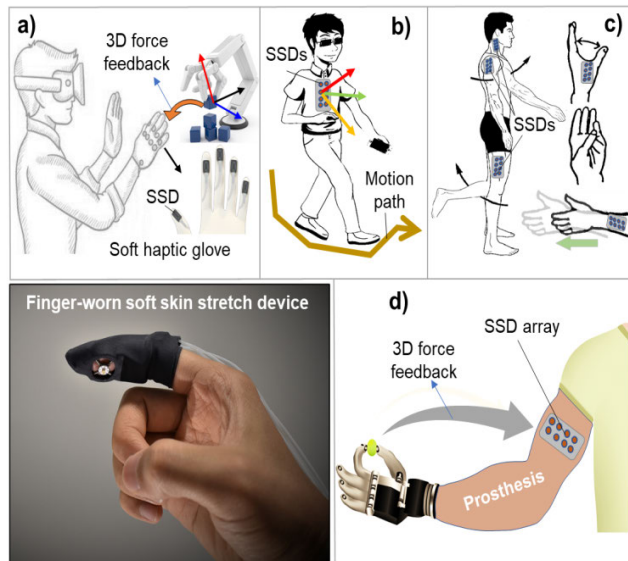

FIGURE 1. Potential application areas of soft skin stretch devices (SSD). a) haptic feedback for teleoperation system, b) navigational assistance for the visually impaired or older people, c) haptic motion guidance for human limbs and body, d) 3D force feedback display for a prosthesis.

To overcome these above drawbacks, this paper will design, fabricate and evaluate a novel SMM and hand worn hydraulic SSDs (Fig. 1). The developed SSDs are integrated into flexible fabrics to enhance the interaction between the device and human skin, similar to human clothing. In addition, SSDs can simultaneously induce omnidirectional shear forces in *x-y* plane driven by four SMMs and a normal *z*-axis force to the contact skin via an adjustable soft tactor. The developed SMM and SSDs will be experimentally characterized and evaluated in different testing modes. To control the force threshold to the SMMs, an initial pre-set elongation (iPSE) mechanism will also be introduced and validated. The magnitude of the generated shear force from the SSD and SMMs as well as the working area of the tactor head will be tested in different directions.

The rest of this paper is organized as follows: Section II presents the design and fabrication for a new hydraulic source-driven SMM, followed by an analytical model for the output force and motion with respect to the applied input pressure. This section will also include the characterization of the SMM in elongation, force and durability tests. Section III gives the design and fabrication of 3-axis SSDs

with a kinematic model within its working space. This section also introduces the characterization, real-time validations and data analyses for the soft 3-axis SSDs. Finally, discussion, conclusion and future works are drawn in Section IV.

II. DESIGN CONCEPT, FABRICATION, MODELLING AND EVALUATION
This section will introduce the design, fabrication, modelling and evaluation of the SMM towards the development and soft 3-axis SSDs for various wearable haptic applications.

A. DESIGN, FABRICATION OF SOFT MICROTUBULE MUSCLE
Existing actuators such as electromagnetic actuators, hydraulic pistons, tendon-sheath mechanisms, piezoelectric actuators, dielectric actuators are inappropriate as hand-worn SSDs due to the occlusion by rigid components that are not able to match with the geometric complexity of the skin's surface or low forces needed to effectively induce the SS sensation. In this section, we will develop a new type of muscle that can transmit force and motion from a distance without sacrificing its input energy. The developed SMM presented in this work is driven by a fluid pressure source that consists of a flexible silicone microtube and a hollow micro-coil which is made from inextensible fibers. The obtained muscle composite is lengthened or shortened under the applied fluid pressure. A fluid transmission tube or guide tube which connects the inner channel of the soft microtubule to a miniature syringe and a micro DC motor (Faulhaber, Germany) via a linear ball screw system (MISUMI, Japan) is used to supply the pressure. By constraining the radial expansion of the flexible microtubule with the micro-coil, it is possible to mechanically program the muscle to perform desired motions and forces. The fabrication process for the SMM is shown in Fig. 2. In this paper, we use flexible silicone microtubules which were successfully fabricated in our previous work [29]–[31]. The obtained microtubule is inserted into a hollow micro-coil made from inextensible fibers. The micro-coil that we use here are a type of stainless-steel micro-coil that can store elastic energy under the applied strain. Once the soft microtubule is completely inserted into the coil, one end is tied into a knot and permanently adhered onto the coil end by an adhesive glue (LOCTITE®, USA) while the other end is connected to a commercial fluid tube (Cole-Parmer, USA). The fluid transmission tube is then connected to a miniature syringe via a blunt needle. To remove the air bubbles that are trapped inside the soft silicone microtubule and fluid transmission tube, the entire structure is degassed in a vacuum chamber for 30 minutes (Binder - VD115, Binder, USA) until the air bubbles have completely disappeared. When fluid pressure is applied to the actuation channel, the SMM will be lengthened from position A at length L_0 to position B at length L with a displacement x which is due to the circumferential constraint by inextensible fibers around the microtubule channel. At point B, the muscle stores elastic energy. If a load is connected to the end of the SMM at

position B and the fluid is removed, the stored elastic energy is released, allowing the muscle to apply a force against the load and bring it back to the position A with a displacement x. The higher pressure that is applied, the higher elastic energy that is stored and thus a higher contraction force is achieved.
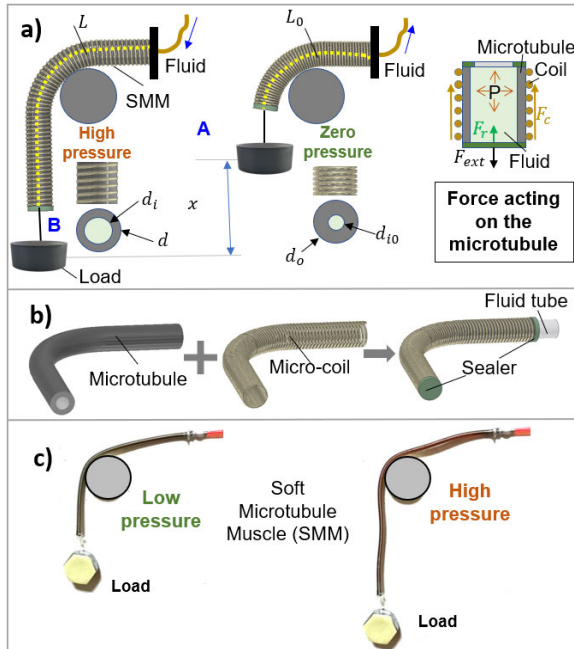

FIGURE 2. Soft microtubule muscle (SMM). a) working principle where L_0 is the initial length of the muscle, L is intermediate length of the muscle with respect to intermediate applied pressure P; b) fabrication process for the SMM; c) obtained prototype for the soft muscle at low applied pressure and high applied fluid pressure.

In our prototype, the flexible silicone microtubule has an outer diameter of 1.1 mm, an inner diameter of 0.7 mm and a working length of 50 mm. It is noted that the developed SMM is scalable and therefore its diameters and length can be varied to adapt to specific applications. The constrained coil has an outer diameter of 1.5 mm, an inner diameter of 1.1 mm and the micro-coil wire (stainless steel) has a diameter of 0.1 mm that covers the entire length of the silicone microtube. The coil material can be fabricated from any inextensible fibers with high flexibility and low weight. The use of stainless-steel coils offers many advantages including high durability and high energy storage compared to other alternatives such as fishing line, sewing thread or nylon coils.

B. ANALYTICAL MODEL FOR THE SMM

To model the developed soft microtubule actuator, we assume that the water pressure is uniformly applied to the inner channel and there are no radial expansions during the operation. We also use 0.5 as the Poisson's ratio for the soft silicone microtubule with an assumption that the material volume of the silicone tube is constant during its working period. With these assumptions, the cross-sectional area of the silicone microtubule before and after the applied fluid pressure can

be expressed by:

$$\pi(d_o^2 - d_i^2)(1 + \varepsilon_l) = \pi(d_o^2 - d_{i0}^2), \tag{1}$$

where d, d_i, are the outer diameter, inner diameter during the working period and d_{i0}, d_o are the inner diameter and outer diameter at the initial state of the silicone tube, respectively. ε_l is the strain in the axial direction.

In the axial direction, the total elastic force in the coil F_c and the tubing F_r is balanced by an external force (load), F_{ext}, dissipative forces, F_{dis}, include viscosity and friction and the force due to the pressure inside the muscle, F_p:

$$F_{ext} = F_c + F_r - F_p + F_{dis} \tag{2}$$

The elastic force in the coil is given in (3) where x denotes the elongation of the muscle and k_c is the stiffness of the constraining coil.

$$F_c = k_c x \tag{3}$$

The elastic force in the silicone microtubule can be expressed by [32]:

$$F_r = EA_{d0}\left(1 - \frac{1}{1 + x/L_0}\right) \tag{4}$$

where, $A_d = 0.25\pi(d^2 - d_i^2)$, $A_{d0} = 0.25\pi(d_o^2 - d_{i0}^2)$, E is Young's modulus and L_0 is the unstretched length of the muscle.

The driving force F_p can be expressed by:

$$F_p = A_{di}P = 0.25\pi d_i^2 P \tag{5}$$

where P is the fluidic pressure inside the microtubule channel and fluid transmission tube.

The dissipative forces, F_{dis}, include hydrodynamic flow resistance, $F_{dis,hyd}$, and dry friction at the tube fabric interface, $F_{dis,dry}$ as shown in [33]:

$$F_{dis} = F_{dis,hyd} + F_{dis,dry} \tag{6}$$

However, $F_{dis,hyd}$ and $F_{dis,dry}$ can be neglected under the assumption that the relative motion of the tube and the coil is small and the muscle is operating in quasi-hydrostatic operation. Therefore, the net external force exerted by the SMM is:

$$F_{ext} = F_c + F_r - F_p = k_c x + EA_{d0}\left(1 - \frac{1}{1 + x/L_0}\right) - A_{di}P \tag{7}$$

The force applied to a load or external force F_{ext} in reverse motion achieves its maximum value at maximum elongation x_{max} with applied pressure $P = 0$. This maximum value is extremely important in our skin-stretch design, which determines how much force is applied to the tactor head. At a certain fluid pressure, P, the muscle elongates to a distance, x, and $F_{ext} = 0$, at this pressure, the relationship between elongation distance and fluid pressure can be found:

$$P = \frac{k_c x^2 + k_c L_0 x + EA_{d0} x}{A_{d0} L_0} \tag{8}$$

Assume that all mechanical energy from the syringe plunger, W_p is transferred to the elastic energy of the coil, W_c and the silicone tube, W_r and the energy lost, W_l, due to sliding friction through the working fluid. Mechanical energy from the syringe plunger is equal to work generated in the fluid system. The energy relation can be given by:

$$W_p = W_c + W_r + W_l \tag{9}$$

$$PV = \frac{1}{2}k_c x^2 + \frac{1}{2}k_r x^2 + W_l \tag{10}$$

where V is the volume of fluid that is pushed into the actuator, and k_r is the instantaneous spring constant of the rubber tubing with the equation as shown in [32]:

$$k_r = \frac{EA_{d0}L_0}{(L_0 + x)^2} \tag{11}$$

Finally, we get the relationship between the liquid volume and the elongation of the actuator.

$$V = \frac{\frac{1}{2}k_c x^2 + \frac{1}{2}k_r x^2 + W_l}{P} \tag{12}$$

The experimental characterization of the total amount of energy lost due to the non-linear characteristics is beyond the scope of this paper. In the later sections, we compared the actual results and the predictions of the above analytical model with the geometric dimensions of each component and mechanical parameters from our measurements such as $k_c = 9.902$ N/m, $E = 1.3$ MPa, $A_{d0} = 2.26 \times 10^{-6}$ m^2, $L_0 = 45$ mm.

C. CHARACTERIZATION AND DATA ANALYSIS FOR THE SOFT MICROTUBULE MUSCLE

In this section, the characterization and analysis for the SMM in terms of elongation and generated forces with respect to the applied fluid pressure will be carried out. We will also evaluate the performance of two SMMs connected in an axial configuration via a tactor head. The maximum displacement and velocity of the tactor will be also introduced.

1) ELONGATION TEST

An elongation test is performed using an apparatus as shown in Fig. 3a. One end of the microtubule is fixed on a 3D printed base while the other end is connected to a constant load of a force 0.1 N via an optical encoder (S6S-1000-IB, US Digital, USA) to record the position of the SMM distal end. The working fluid was supplied via BD Luer-Lok$^{\text{TM}}$1-mL syringe (inner diameter of 4.5 mm) driven by a DC micromotor (model 3272G024CR with encoder IE3-1024, Faulhaber, Germany) and a ball screw mechanism (MISUMI, Japan). To mitigate the nonlinear hysteresis from the DC gearhead and ball screw system, we use another optical encoder (S6S-1000-IB, US Digital, USA) to record the displacement of the syringe plunger. Fluid pressure is monitored using a pressure sensor (40PC Series Sensor, Honeywell, USA). To eliminate the pressure loss during the operation, the pressure sensor
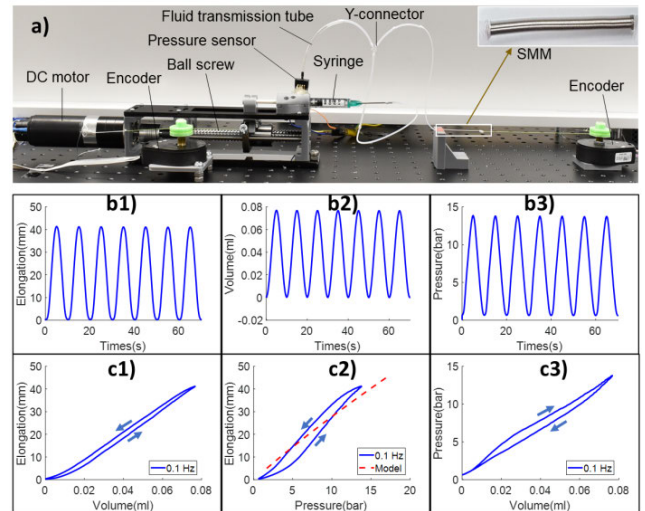

FIGURE 3. Elongation test. a) apparatus for elongation testing. b-c) results of elongation versus volume and pressure showed consistent performance over repeated actuation and comparison between the measured data and the developed analytical model.

is located as close as possible to the muscle port via a Y-connector. The soft muscle is driven by a sinusoidal fluid displacement at a frequency of 0.1 Hz (slow motion for skin stretch applications) while the fluid pressure is varied from 1 bar to 15 bar. The signals are decoded synchronously using a data acquisition device (QPIDe Data Acquisition Device, QUANSER, Canada) and MATLAB Simulink (Mathworks, Inc., USA). The signal from the pressure sensor is passed through a digital lowpass filter to eliminate high-frequency noise [34], [35]. The instantaneous displacement of the fluid volume is calculated from the displacement of the syringe plunger and its geometry.

The experimental results (Fig. 3) show that the muscle elongation increases with additional fluid volume or applied fluid pressure by moving the syringe plunger forward and vice versa for the reverse motion. This response is consistent with the elongation and fluid pressure under repeated actuation. It is noted that the relation between volume and displacement is almost linear with a small hysteresis loop while the volume-pressure and pressure-elongation relationships exhibit greater hysteresis. A notable divergence from the developed model and experimental data is a nonlinear hysteresis due to the deformation of nonlinearly elastic materials and friction loss that are not taken into consideration in (1) to (12). A more accurate model is needed to give a better understanding of the muscle response. However, in this paper, we only investigate the design and fabrication of the new muscle and therefore a complicated model is reserved for future work. However, the developed analytical model correctly predicted the observed ranges of muscle elongation and the data which means that the muscle performance is within the expected range that is demonstrated by a closer trend of the model to follow the real experimental data (see Fig. 3c2) and even in the higher frequency of fluid movement.

There is a small hysteresis loop from the relation between applied input volume or displacement motion of the syringe plunger. This advantage opens a great opportunity for feed-forward or feedback control [36], [37] when the displacement or volume is used as control input compared to that of pressure with a wider hysteresis loop. Therefore, our future work on precise motion control of the developed muscle will consider this observation.
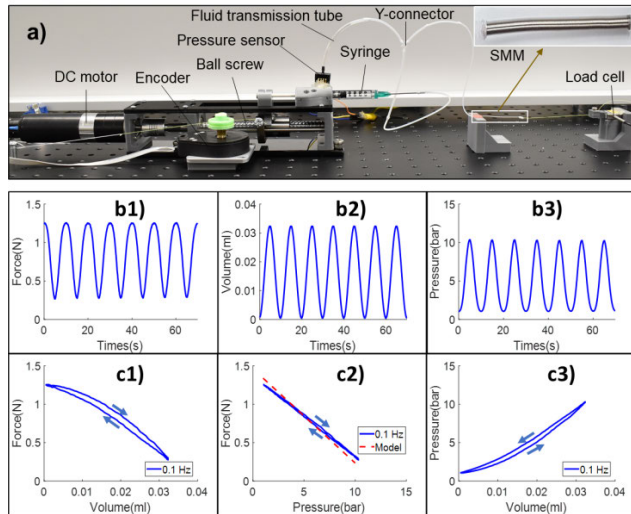

FIGURE 4. Axial force testing. a) Apparatus for axial force testing. b-c) Results of force, volume and pressure showed consistent performance over repeated actuation and comparison between the measured data and the developed analytical model.

2) AXIAL FORCE TEST

We also evaluate the force performance of the SMM in the axial direction using an experimental setup given by Fig. 4a. To record the force response, a miniature FUTEK load cell (1 lb, FUTEK, USA) is used. One end of the SMM is fixed on a 3D printed base while the other end is connected to the load cell head which is mounted onto a 3D printed platform. The applied input from the miniature syringe to the muscle is similar to that of elongation tests. Results indicate that the SMM performs consistently over repeated testing cycles. Particularly, the force-pressure curve exhibits a linear relation with a small nonlinear hysteresis loop while the force-volume and pressure-volume introduce a higher hysteresis nonlinearity. The analytical models given by (1) to (12) reveal a qualitatively good agreement with the experimental data (Fig. 4c2). This means that in the force mode control, the pressure can be used as control input instead of fluid volume or plunger displacement. In addition, the pressure information can be used to provide a good prediction of the output force under the absence of an onboard force sensor. This plays a vital role in the development of SMM-based compact wearable haptic devices and other applications where the use of bulky components to provide the output feedback is avoided. The hysteresis loops for the force-volume and pressure-volume curves show a strong nonlinearity in both forward and backward directions. A precise nonlinear dynamic model that can

capture these hysteresis effects is desired to provide a better understanding of the developed SMM for both motion and force mode operation.

3) PERFORMANCE CAPABILITY OF SMM

We also carry out experiments to examine the maximum elongation of the SMMs so that they have appropriate specifications for our developed SSDs and other wearable haptic and assistive systems. The experimental setup and size of SMM are similar to that used in the elongation and force tests. To determine the maximum elongation level, we first increase the fluid volume from a miniature syringe to the SMM until it fails. While the soft microtubule alone has high elongation at its breaking point, the maximum elongation of the SMM highly depends on the outer micro-coil (size of fibers and the coil pitch). Our experimental results show that the flexible silicone microtube has a high elongation at break of 750% (Ecoflex-0030) while the constrained micro-coil only elongate up to 200% (we performed 10 trials and the presented result is mean value). However, we observe that most failures originate from the sealer and connector at both ends of the SMM. This can be explained by a weak interface between the rigid components (fluid transmission tube) and soft materials (silicone microtubule). To ensure that the failure does not originate from these mechanical factors, a stronger adhesive sealer at the connectors is highly desirable. We anticipate that our SMM strain can reach the elongation limit of the micro-coil until ballooning occurs in between the two ends of the SMM due to the silicone microtube reaching its elastic material limit under high applied stress and strain contingent on the fact that the connectors and sealers are sufficiently strong to maintain the contact. However, our developed SSDs only require approximately 1 mm to move the tactor and induce a desired SS sensation and therefore an elongation of approximately 100% is sufficient. To determine the soft muscle length used in our SSDs, experiments with trials and errors were carried out before the fabrication of the SSDs.

We also investigated and validated the relationship between the elongation and the corresponding maximum force in real experiments and compare the obtained measured data and our developed model given by (8). The comparison result is given in Fig. 5. Here, we select an initial length of around 45 mm plus 20 mm for each soft muscle to be used in the SSDs as it can generate a sufficient tangential force (around 1N as shown in the literature [38]) in order to induce a shear force sensation to the human skin at the finger. The result reveals that the actual data is close to the developed model, but the maximum force obtained from the developed model is slightly higher than that of the measured data. This can be attributed to the loss caused by sliding friction and the dissipative energy in the experiment that our models do not take into consideration.

4) DURABILITY TEST

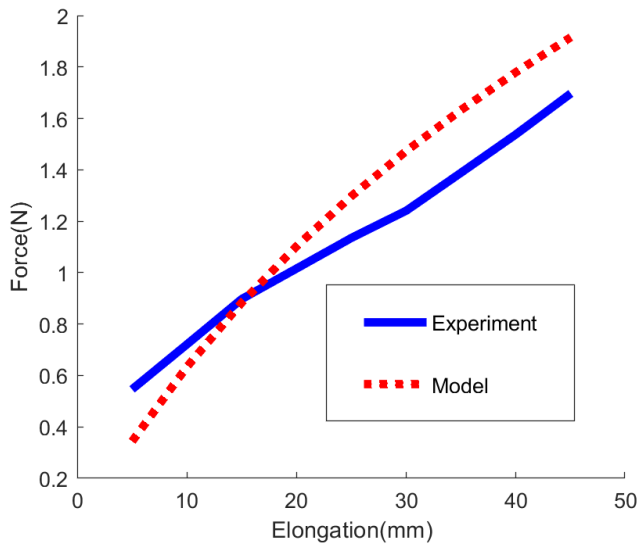We also carried out experiments to evaluate the SMM durability over time in order to ensure that the performance of

FIGURE 5. The relationship between the elongation and the maximum force in the model and the actual experiment.
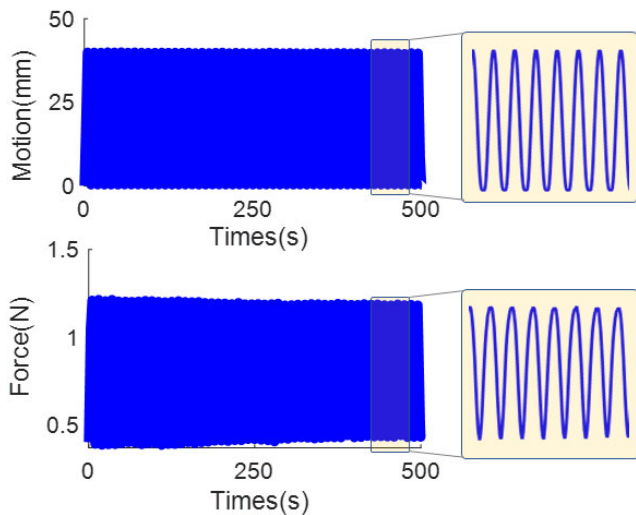

FIGURE 6. Durability test for both motion (upper panel) and force (lower panel) of the SMM.

the SMM-based SSD is stable during its operation (Fig. 6). A sinusoidal signal is applied for each test (elongation and force) until the SMM reached a maximum elongation of 40 mm and a maximum force of 1.2 N, respectively. The performance of the soft actuator was consistent over the testing period although there is an approximate 0.4% reduction in the elongation and a 5% reduction in the axial force. This reduction can be attributed to the stress relaxation of the inner elastic tube, so we could conclude that this device can provide a roughly similar skin-stretch effect on fingertip skin after many cycles.

III. DESIGN, FABRICATION AND MODELLING OF THE 3-AXIS SKIN STRETCH DEVICES
A. WORKING PRINCIPLE OF THE SOFT 3-AXIS SKIN STRETCH DEVICE

Most existing SSDs are rigid and therefore they are not able to conform to the human skin to induce effective shear forces,

which prevent their use in many haptic applications. To overcome these limitations, we have developed a new soft 3-axis SSD where the shear forces (F_x, F_y) to the skin are controlled by four SMMs. To deliver accurate SS sensation to the skin, a normal force F_z in the z-axis driven by a soft adjustable tactor is used. The new SMMs-driven 3-axis SSD consists of four SMMs, a soft tactor, a wearable fabric housing, initial pre-set elongation (iPSE) mechanisms and outer sheaths as shown in Fig. 7. The technical specifications of our developed device are given in TABLE 1.
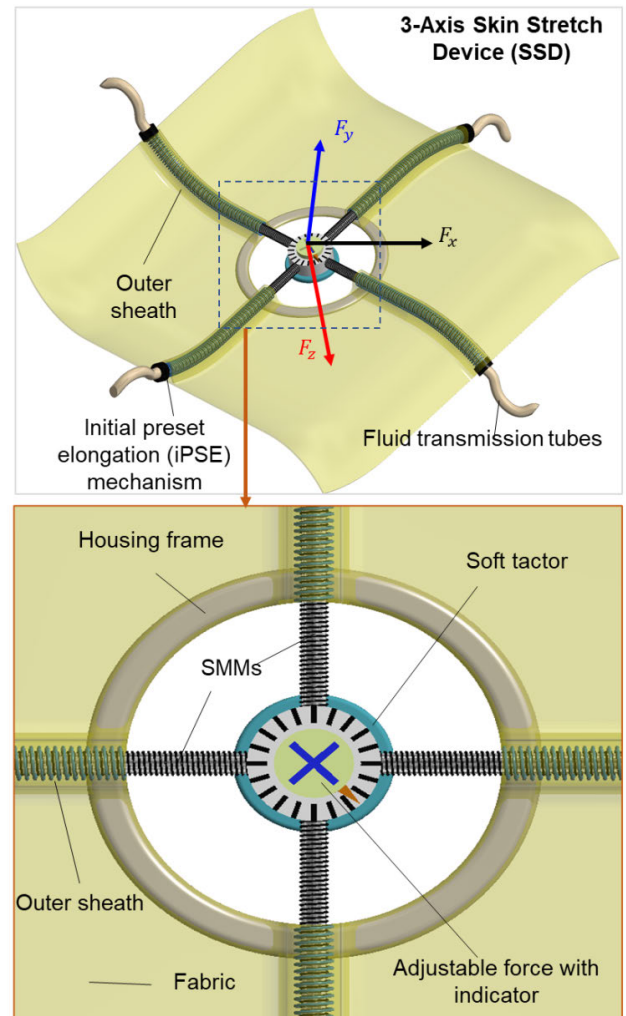

FIGURE 7. SMMs-Driven 3-Axis Skin Stretch Device Integrated into Flexible Fabrics with indication of applied force directions, adjustable soft tactor with indicator, outer sheath and flexible fabric as interface.

To enhance the interaction between the device and the wearers, SSDs will be integrated into a flexible fabric layer that allows the devices to be worn like human clothing. The sliding tactor is made from soft silicone elastomer (composite between Sylgard 184, Down Corning and Ecoflex 0030, Smooth-On Inc.) to enhance the interaction force between the SSDs and the user's skin. The tactor, which is connected to the four SMMs, can slide over the skin surface to induce the skin stretch sensation. The relative position of the tactor

with respect to the fabric housing is controlled by miniature syringes remotely located far away from the working areas via the four SMMs which are arranged in a cross shape where the tactor head is used as a 4-way connector. At the beginning of the assembly, each SMM is elongated to reach a level of 50% of its maximum strain so that a balancing force is maintained. To control the motion in the desired direction, individual SMMs are controlled in pressurized, depressurized or initial states, depending on the movement of its associated syringe plunger. By controlling the pressures applied to the muscles, we are able to control the tactor position within the working space r_w as well as normal force to the skin by adjustable tactor head. For example, at the center (position G, Fig. 8b), pressures $P_1 = P_2 = P_3 = P_4 = P_0$ and contraction forces generated by the SMM are balanced $\overrightarrow{F_{P1}} = \overrightarrow{F_{P2}} = \overrightarrow{F_{P3}} = \overrightarrow{F_{P4}}$, while at the position H, the applied pressures to the SMMs $P_1 < P_2, P_3, P_4$ with their contraction forces $\overrightarrow{F_{P1}} = \overrightarrow{F_{P2}} + \overrightarrow{F_{P3}} + \overrightarrow{F_{P4}}$ (Fig. 8d). At position I, Fig. 8c, $P_1, P_4 < P_2, P_3$, and therefore the SMM forces are $\overrightarrow{F_{P1}} + \overrightarrow{F_{P4}} = \overrightarrow{F_{P2}} + \overrightarrow{F_{P3}}$. Note that P_0 is the balanced pressure applied to the SMMs when the tactor is located in the center of the working space with radius r_w and P_1, P_2, P_3, P_4 are the pressures inside the SMM 1, 2, 3, 4, respectively. $F_{P1}, F_{P2}, F_{P3}, F_{P4}$ are the contraction forces produced by SMMs 1, 2, 3, 4, respectively.
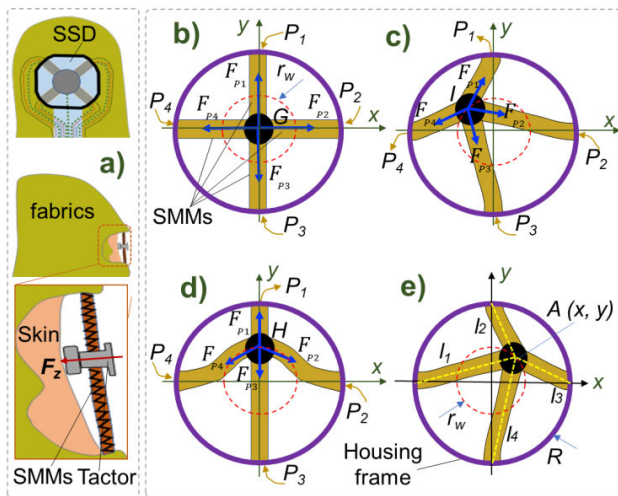

FIGURE 8. Working principle of the 3-axis skin stretch device (SSD). a) SSD on user's fingertip with fabric layer; b) tactor head at the balanced state; c, d) motion of the tactor controlled by the four SMMs; e) calculation for the SMM length with respect to tactor location.

B. IPSE: INITIAL PRE-SET ELONGATION

One of the main advantages of our SSDs is the ability to control the generated force or displacement threshold while maintaining the muscle length at a fixed value via the use of the initial pre-set elongation (iPSE). To create an efficient and comfortable wearable SSD, the movement area of the tactor head should be maximized while its size is minimized. Several factors such as the contraction force from the SMMs

and the elongation of their associated opposite SMMs can affect the tactor motion. To characterize the effect of iPSE on the tactor displacement, we fabricate 1-axis SSDs which consist of a tactor and two SMMs (Fig. 9). We perform twenty experiments and each experiment is carried out with different 1-axis SSD at different iPSE values for each SMM but a fixed nominal length for the device or ($L_{01} + L_{03}$) is maintained. The working range of each SDD is defined by the total length of the two SMMs ($L_{01} + L_{03}$) which are connected via a tactor (see Fig. 9). As an illustration, the displacement of the tactor given in Fig. 9b (high iPSE) is greater than that of Fig. 9a (low iPSE).
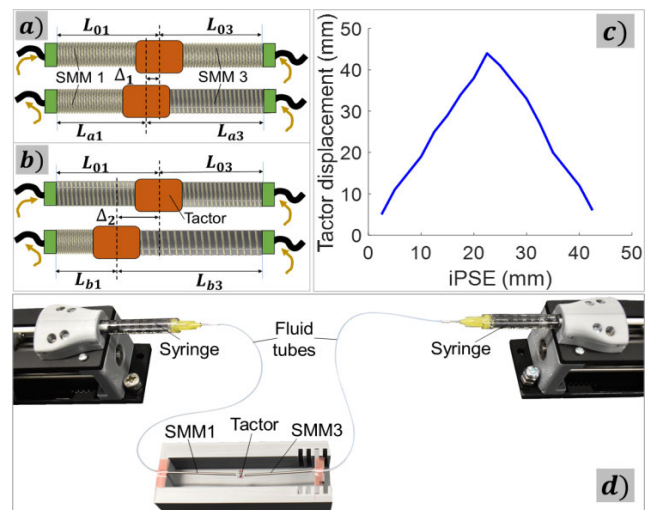

FIGURE 9. Evaluation for Initial Pre-Set Elongation. a, b) Different tactor displacement of the 1-axis SSD with different initial elongation of the SMMs; c) experimental result (tactor displacement versus iPSE) for the maximum displacement of the tactor head attached into two soft muscles for various iPSE values; d) experimental setup with two DC-motors-driven 1-axis SSD.

TABLE 1. Main features of soft microtubule muscles-driven 3-axis SSD.

Overall Dimension for the SSD	Outer frame diameter (12 mm), thickness including fabric layer (2 mm)
Weight	4.3 g
Number of degrees of freedom	3
Motion range of the tactor	Up to 9 mm in diameter of the circular trajectory
Force	Up to 1.8 N
Max speed	20.14 mm/s
Max elongation of each muscle	100%

For each experiment, we use a 5% increment of the elongation for the SMM. To measure the tactor head position, we use a laser displacement sensor (Model IL-100, Keyence, USA) which is connected to a controller (QPIDe, Quanser, Canada). Fig. 9c gives the experimental result for the maximum displacements of the tactor head which corresponds to each iPSE value. The result reveals that the optimal iPSE value for our current design is 150% that will be used as an input value

for our developed 3-axis SSDs. Beyond this value, the tactor displacement is decreased which can be explained by the limitation on the elastic strength of the silicone microtube and the outer micro-coil elongation.

To implement the optimal iPSE into SSDs in practice, we first elongate each SMM up to 50% of its optimal iPSE value. This point is defined as an initial starting position for the tactor or its balanced position. The control strategy to move the tactor to the desired position and orientation is given in Fig. 8. The skin stretch velocity is one of the main factors for mechanoreceptor discharge rates [39]. Therefore, we also examine the maximum speed of tactor head movement at maximum iPSE value for SMMs (∼150% elongation). The speeds are recorded using a Keyence displacement sensor. We performed 10 trials with the highest velocity applied to the DC motors-driven miniature syringes by withdrawing the fluid in one SMM while adding the fluid into the other SMM. Results show that the average speed is approximately 12.30 mm/s while the maximum speed is 20.14 mm/s.

It is noted that the SMMs used in real-time experiments are buckled if the lengthened ones exceed a threshold beyond their balanced position. To better describe this phenomenon, we analyze the balanced force and applied pressure to the tactor (see Fig. 9a) or $F_{P1} + F_{P3}$ and adjust pressures $P_1 = P_3 = P_0$. Experimental data show that if the applied pressure to SMM1 or SMM3 is increased to a value that is higher than a threshold (P_1 or $P_3 > P_0$), unexpected buckling occurs in the depressurized muscle (SMM1 or SMM3). As the SMMs are controlled by independent syringes while our SSD is working in open-loop mode, it is challenging to control the opposite SMMs to the desired position. In order to avoid this unexpected buckling, we use a pressure threshold for each actuated SMMs so that the DC motors can be controlled within this threshold. The future work will implement closed-loop control so that buckling is completely eliminated.

C. FABRICATION OF OUTER SHEATH AND IPSE MECHANISM

To guide the SMMs within the fabric layers, outer sheath mechanisms are needed. The sheath mechanism is a type of hollow plastic coil springs that are made from the 0.5 mm fishing line (Jarvis Walker, Australia). To fabricate the outer sheath, we wrap the fishing line around a carbon fiber rod (1.43 mm in outer diameter, CST, Composite Store Inc., CA, USA) using a hand drill machine as shown in Fig. 10. To maintain the helical shape, we place the composite into an oven at 130°C for 2 hours. Next, we use a hollow carbon fiber rod (inner diameter of 1.5 mm, CST, Composite Store Inc., CA, USA) to release the coil. Only uniform coils are chosen for use in our wearable haptic device. To adjust the iPSE value for the SMMs, we also develop an iPSE mechanism that consists of an actuator holder and spacers. As the fishing coil and SMMs are highly flexible, they can be easily integrated into the fabric layers so that users do not have any discomfort with rigid components.
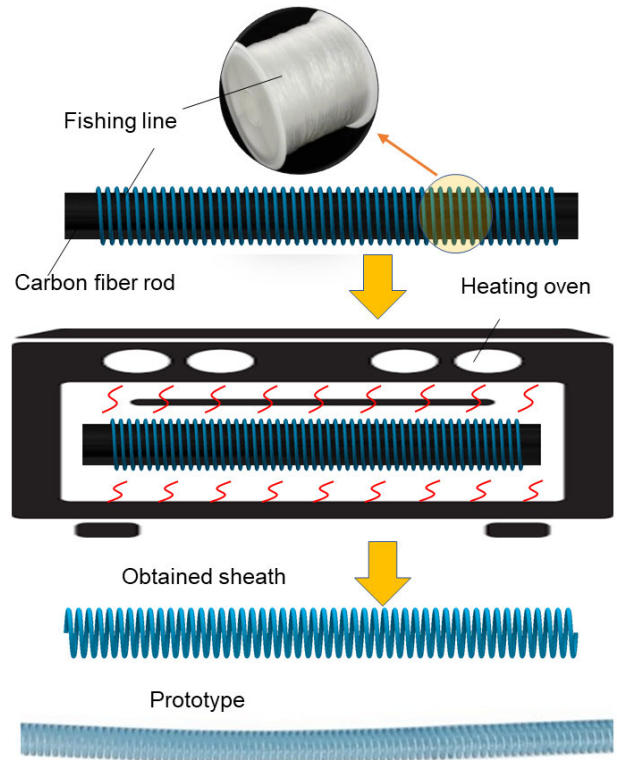

FIGURE 10. Fabrication process for the outer sheath.

D. KINEMATIC MODEL OF THE SSD TACTOR

To characterize the SSD tactor, we introduce a kinematic model that represents the relationship between the position of tactor A (x, y) and the working length of each SMM l_1, l_2, l_3, l_4 within the housing frame R as shown in Fig. 8e.

The tactor head only reaches the radius of $r_w < R$ due to the constraint of this frame, the size of SMMs and the tactor radius. The working length of each SMM within a radius R is expressed by:

$$\begin{cases} l_1 = \sqrt{y^2 + (x+R)^2} \\ l_2 = \sqrt{x^2 + (R-y)^2} \\ l_3 = \sqrt{y^2 + (R-x)^2} \\ l_4 = \sqrt{x^2 + (y+R)^2} \end{cases} \Rightarrow \begin{cases} l_1 = \sqrt{\Delta + 2Rx} \\ l_2 = \sqrt{\Delta - 2Ry} \\ l_3 = \sqrt{\Delta - 2Rx} \\ l_4 = \sqrt{\Delta + 2Ry} \end{cases} \quad (13)$$

where $\Delta = R^2 + x^2 + y^2$

The actual length of each SMM (L_{mi}), $i = 1, 2, 3, 4$ which depends on the tactor position at A (x, y) is given by:

$$\begin{cases} L_{m1} = L_0 - (R - l_1) \\ L_{m2} = L_0 - (R - l_2) \\ L_{m3} = L_0 - (R - l_3) \\ L_{m4} = L_0 - (R - l_4) \end{cases} \quad (14)$$

where L_0 is the initial length of each SMM.

One unique design in our SSD is that each SMM slides inside a hollow coil as a sheath embedded into flexible

fabrics. This enables the SMM to be controlled by a remote external hydraulic source through long, narrow and tortuous paths, eliminating bulky on-board actuators and allowing the compact design of a simpler and smaller haptic device for the fingertip [40]. Although this configuration is inspired by the tendon-sheath mechanism [41], our proposed approach offers better performance in terms of energy efficiency due to the smaller loss of nonlinear friction and hysteresis (See Fig. 3 and Fig. 4). Our design does not limit the motion of the wearer because the housing is made from flexible fabric that is highly conformal and adaptable to the skin surface. In addition, the developed device is compact and lightweight and therefore it does not prevent relative movement of the fingers during the operation. These features are challenging to obtain by current haptic devices available in the literature.

FIGURE 11. Four SMMs-driven 2-axis SSD integrated into flexible fabric layers.

E. SMMS-DRIVEN 2-AXIS SKIN STRETCH DEVICE

It has been shown that the skin stretch feedback is capable of conveying position and spatial direction via a small tactor, just a few millimeters in diameter [42]. When we lift an object, the perception of the weight of the vessel is primarily mediated by cutaneous afferents that sense the strain of the skin. The motions and velocities required to impart skin stretch can be slow, allowing the design of compact, low power and portable devices. To meet the displacement requirement for cutaneous haptic feedback, we further investigate the capability of the SSD tactor for directional and positional cues. We fabricate four SMMs-driven 2-axis SSDs with an optimal iPSE value of 100% for the muscles (Fig. 11) where four DC micromotors (model 3272G024CR with encoder IE3-1024, Faulhaber, Germany) connected to ball screw mechanisms (MISUMI, Japan) are used to control the SMMs via BD Luer-Lok^{TM} 1-mL syringes. Fluid pressure is monitored using pressure sensors (40PC Series Sensor, Honeywell, USA). We perform experiments with a maximum displacement of tactor within its working area via the evaluation of its reachability for eight different directions. Results given in Fig. 12 show that the tactor head is able to reach a target position in desired directions. It is noted that the tactor can reach a circle of 9 mm within the working area of 10 mm in diameter. This demonstrates that our SSD tactor can achieve 90% of the theoretical working area.

We also evaluate the tracking capability of the developed 2-axis SSDs to follow desired circular trajectories with a diameter of 1.6 and 3 mm in the x-y plane which is tangential to the skin surface. In this experiment, four SMMs are simultaneously controlled by the four DC micromotors via syringe systems in an open-loop mode which is based on the kinematic model given by (14). We used a camera (Logitech HD Pro Webcam C270) with $1280 \times 720p$ resolution to record the experiment. We developed a video processing code in Matlab Simulink (MathWorks, Inc., USA) to track the tactor position. Although the results given by Fig. 13 show that the SSD tactor can follow the desired trajectory under the constraint of the kinematic model, there still exists a tracking error that prevents the tactor to precisely follow the desired trajectories. Therefore, we recommend using a closed-loop controller with advanced nonlinear hysteresis model and online adaptive feedback [43] to track the desired trajectory perfectly. This will be considered in our future work.
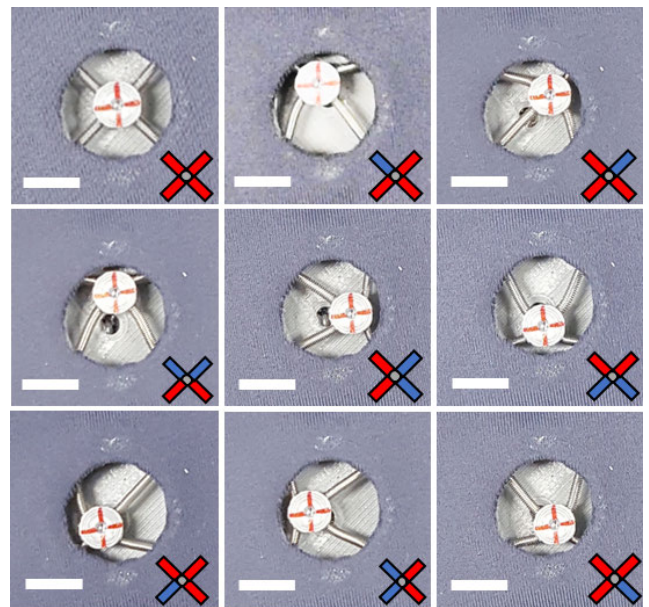

FIGURE 12. Various positions of the tactor head achieved by controlling the extension of four SMMs. In the bottom right-hand corner of each image, the pressurized muscles are shown in red and the depressurized muscles are shown in blue. Scale bar: 5 mm.

F. SHEAR FORCE MEASUREMENT

We also measured the magnitude of the shear force induced by the soft tactor in eight different directions. We use 100% for the iPSE value in this experiment. A FUTEK loadcell 1 lb (FUTEK, USA) is used to monitor the force signal. To generate the force to the tactor, we use similar control architecture as that of Fig. 11. The maximum shear forces in eight directions are shown in Fig. 14. The results show that the shear forces along diagonals are higher than that of the principal directions. This can be explained by the fact that two adjacent muscles generate a higher force compared to a single one. The shear forces in the opposing directions
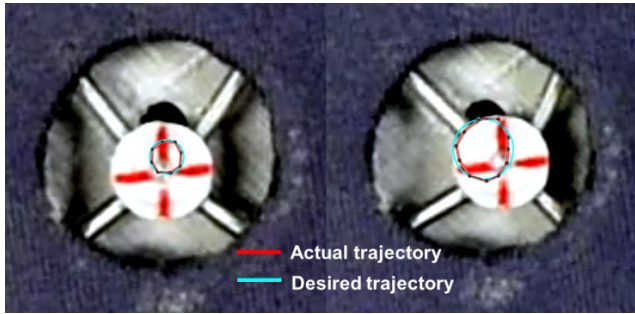
FIGURE 13. Tracking capability of the tactor in the 2-axis skin stretch device with a tracking circle of 1.6 mm (left panel) and 3 mm (right panel) in diameter.
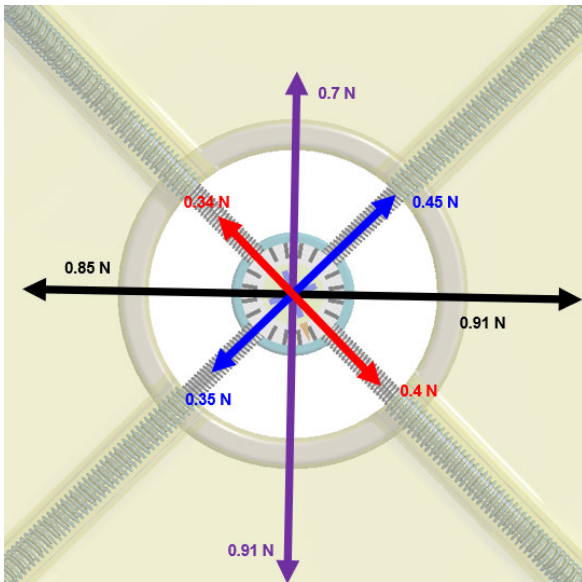

FIGURE 14. The maximum shear force for SSD in eight directions.

are likely different because of intrinsic inconsistencies in the fabrication process by hand. This unexpected factor can be alleviated by using the iPSE mechanism with adjustable spacers in order to make ensure the shear forces in the major axes are roughly similar at the beginning.

G. 3-AXIS SSD WITH SOFT TACTOR

In our developed SSDs, the tactor plays a vital part to connect the four SMMs and to induce stretch sensation to the skin. Prior studies have shown that the human perception of shear force is proportional to the magnitude of the normal force applied [38]. To deliver accurate haptic stimuli to the skin, it is essential to control the mechanical contact state which is especially challenging for current SSDs. Adhesion of the tactor with the skin will thus be achieved via a soft silicone surface. In order to control the normal force F_z in the z-axis, an adjustable mechanism is used. The soft tactor consists of a soft silicone layer at the bottom connected to the tactor head via a micro bolt. The adjustable tactor can control the strength of contact friction forces, enabling a wide

range of haptic stimuli. With this new design, our SSD is able to impart a directional shear force that can displace, deform and stretch the skin, depending on the application such as textual communication, directional cues for motion guidance and 3D force feedback display. To connect one end of the four SMMs to the tactor base, we use an adhesive glue (LOCTITE®, USA) while the other end is connected to a commercial fluid microtube (Cole-Parmer, USA). The 3D printed base is designed in a way that aligns the four force vectors from the SMM in the *x-y* plane. The soft tactor head which is made of ReoFlex 30 urethane rubber (Smooth-On, Inc., USA) provides high friction to improve the effect of skin stretch. The adjustable mechanism is a 3D printed bolt that can travel along the z-axis via a threaded hole in the tactor base. To achieve the desired contact force, users just simply adjust the bolt via its head. This mechanism also possesses an indicator that has a linear relation with the contact force via an adjustable angle of the bolt.
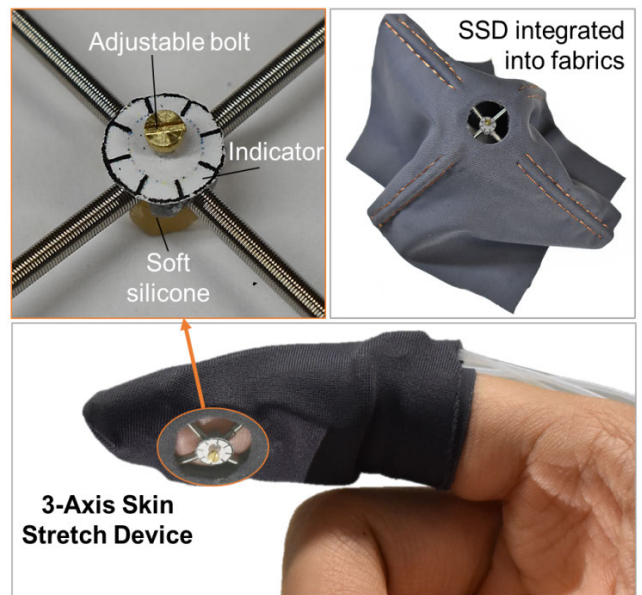

FIGURE 15. Soft 3-axis skin stretch device with soft tactor. (Upper panel) adjustable soft tactor integrated into 3-axis SSD and flexible fabric, (Lower panel) finger worn soft 3-axis SSD with fabric housing.

The developed soft 3-axis SSD and soft tactor are also integrated into the user's finger via a hand-worn device with fabric layers. First, we used sewing threads to adhere to the SSD into fabric layers (Fig. 11, Fig. 15). To obtain a wearable finger device, we patterned another fabric layer in the form of a finger-like shape using a laser cutting machine and then inserted the obtained SSD composite into this fabric finger shape before reversing inside out to have the final device (Fig. 15). The skin-stretch effect of the tactor in each direction was also tested on the fingertip. Experimental results show that the tactor can move more than 1 mm when it is in contact with the users' skin. In addition, users reported that they did not feel any discomfort when wearing the device for 30 minutes. The initial results demonstrate that our soft 3-axis

SSD can be used to effectively induce SS sensation to the fingers.

IV. DISCUSSION, CONCLUSION AND FUTURE WORK

In this work, we introduced new SMMs, conformal and hand worn hydraulic SSDs that can produce three directional forces to the skin. We designed, fabricated and validated a new generation of hydraulic SMMs that are soft, small and compliant. The developed SMMs can adapt to any geometric complexity of the skin surface while maintaining a high force and motion at any length and scale. The novel SMMs can convey desired force and motion from a far distance through flexible fluid transmission tubes, which offer users hands-free from onboard and rigid mechanical components. We also characterized the muscle performances and analyzed the measured data via experiments, including the elongation, force and durability tests under various working conditions. Analytical models for the SMMs were also developed, evaluated and compared with the real-time measured data. Thanks to the combination of a flexible silicone microtube and a hollow micro-coil, the SMM can induce a contraction force up to 1.8 N at an elongation of 100% its original length. The experimental results also showed a good agreement between our proposed model and measured data in both force and elongation mode under various applied fluid pressures. With a small hysteresis loop, we anticipate that our developed SMMs offer precise motion in the future with the feedforward or feedback control. In addition, the experimental data from durability tests confirmed that the SMM performance is stable during the operation. It is noted that our developed SMM provides a stronger force compared to other soft pneumatic and hydraulic actuator with the same size. The main difference is that the generated force from SMM comprises of both storage elastic energy (STE) from the inner soft silicone microtubule and the restoring force from the micro-coil while existing soft actuators solely rely on STE. We used four independent SMMs to control the motion and force of the SSD tactor in *x-y* axes while the normal force in the *z*-axis is driven by an adjustable soft tactor. Because the developed SSDs were fully integrated into textile layers, they allow sufficient flexibility to highly conform to the complex geometry of the skin surface, similar human clothing (see Fig. 11 and Fig. 15). We also optimized the design of SSDs to maximize the tactor displacement, movement speed and force magnitude.

An iPSE mechanism for the SMMs was also introduced to adjust the threshold of generated shear force and tactor displacement for a wide range of haptic applications. We fabricated an adjustable soft tactor that can deliver accurate haptic stimuli to the skin via a silicone surface. The soft tactor enables an effective interaction between the SSDs and the user's skin. The magnitude of the normal force in the *z*-direction is fully controlled by an adjustable mechanism with an indicator that allows a convenient use for the wearers. A kinematic model that shows the relationship between the tactor position and the working length of each SMM was also introduced and validated. The tactor motion was monitored by an optical camera using image processing techniques. Results showed that the SSDs can effectively induce desired shear forces to lateral surfaces, similar to that of fingertip skin. In addition, the SSD tactor could follow different circular trajectories tangential to the skin surface with different working space diameter (1.6 and 3 mm in the *x-y* plane) using an open-loop controller.

Although the developed SMMs and SSDs offer many advantages over the current approaches [44], [45], several drawbacks still exist. First, our SMMs currently only operate in open-loop control with no motion or force feedback. Second, the use of a manually adjustable tactor to control the normal force for the SSD introduces discomfort to the user, especially in real wearable applications. Third, the developed linear analytical models are not able to capture the nonlinear hysteresis in the SMM system and therefore precise model-based control is limited. To this end, our future work will replace the adjustable soft tactor by developing a fluid-driven soft inflatable actuator. The new soft actuator will provide high flexibility to control the normal force to adapt to a wide range of haptic applications. To provide the position feedback, we will integrate a miniature and soft conductive sensor into the SMM surface that can change its resistance under the applied strain. We will also develop a nonlinear hysteresis model and a closed-loop controller for the SMMs in order to enhance the tracking performance for the devices. The control approach will include feedforward and/or nonlinear adaptive scheme-based control algorithms as our previous works on tendon-sheath mechanisms [46]–[49]. As the main scope of this paper is on the design, fabrication, characterization of a new soft muscle and 3-axis SSD, users' evaluations have not been carried out yet. Therefore, we will also involve user studies in future work to validate the proposed approach. In addition, we also plan to implement the developed SSDs in various haptic applications such as haptic motion guidance, navigational assistance for the visually impaired or older people, tactile textual language, 3D force feedback display for use in prosthesis and virtual and augmented reality.

REFERENCES

[1] Y.-C. Lee, J. D. Lee, and L. Ng Boyle, "Visual attention in driving: The effects of cognitive load and visual disruption," *Hum. Factors, J. Hum. Factors Ergonom. Soc.*, vol. 49, no. 4, pp. 721–733, Aug. 2007.

[2] E. Saddik, "The potential of haptics technologies," *IEEE Instrum. Meas. Mag.*, vol. 10, no. 1, pp. 10–17, Feb. 2007.

[3] M. Sreelakshmi and T. D. Subash, "Haptic technology: A comprehensive review on its applications and future prospects," *Mater. Today, Proc.*, vol. 4, no. 2, pp. 4182–4187, 2017.

[4] U. Proske and S. C. Gandevia, "Kinesthetic senses," *Comprehensive Physiol.*, vol. 8, no. 3, pp. 1157–1183, 2011.

[5] C. Pacchierotti, S. Sinclair, M. Solazzi, A. Frisoli, V. Hayward, and D. Prattichizzo, "Wearable haptic systems for the fingertip and the hand: Taxonomy, review, and perspectives," *IEEE Trans. Haptics*, vol. 10, no. 4, pp. 580–600, Oct. 2017.

[6] K. Bark, J. Wheeler, P. Shull, J. Savall, and M. Cutkosky, "Rotational skin stretch feedback: A wearable haptic display for motion," *IEEE Trans. Haptics*, vol. 3, no. 3, pp. 166–176, Jul. 2010.

[7] S. Ullrich and T. Kuhlen, "Haptic palpation for medical simulation in virtual environments," *IEEE Trans. Vis. Comput. Graphics*, vol. 18, no. 4, pp. 617–625, Apr. 2012.

[8] S. Choi and K. J. Kuchenbecker, "Vibrotactile display: Perception, technology, and applications," *Proc. IEEE*, vol. 101, no. 9, pp. 2093–2104, Sep. 2013.

[9] U. Berglund and B. Berglund, "Adaptation and recovery in vibrotactile perception," *Perceptual Motor Skills*, vol. 30, no. 3, pp. 843–853, Jun. 1970.

[10] J. Wheeler, K. Bark, J. Savall, and M. Cutkosky, "Investigation of rotational skin stretch for proprioceptive feedback with application to myoelectric systems," *IEEE Trans. Neural Syst. Rehabil. Eng.*, vol. 18, no. 1, pp. 58–66, Feb. 2010.

[11] K. Bark, J. Wheeler, G. Lee, J. Savall, and M. Cutkosky, "A wearable skin stretch device for haptic feedback," in *Proc. World Haptics - 3rd Joint EuroHaptics Conf. Symp. Haptic Interfaces Virtual Environ. Teleoperator Syst.*, 2009, pp. 464–469.

[12] A. L. Guinan, N. C. Hornbaker, M. N. Montandon, A. J. Doxon, and W. R. Provancher, "Back-to-back skin stretch feedback for communicating five degree-of-freedom direction cues," in *Proc. World Haptics Conf. (WHC)*, Apr. 2013, pp. 13–18.

[13] V. E. Abraira and D. D. Ginty, "The sensory neurons of touch," *Neuron*, vol. 79, no. 4, pp. 618–639, Aug. 2013.

[14] M. Aggravi, F. Pause, P. R. Giordano, and C. Pacchierotti, "Design and evaluation of a wearable haptic device for skin stretch, pressure, and vibrotactile stimuli," *IEEE Robot. Autom. Lett.*, vol. 3, no. 3, pp. 2166–2173, Jul. 2018.

[15] K. Bark, J. W. Wheeler, S. Premakumar, and M. R. Cutkosky, "Comparison of skin stretch and vibrotactile stimulation for feedback of proprioceptive information," in *Proc. Symp. Haptic Interfaces Virtual Environ. Teleoperator Syst.*, Mar. 2008, pp. 71–78.

[16] Z. F. Quek, S. B. Schorr, I. Nisky, W. R. Provancher, and A. M. Okamura, "Sensory substitution using 3-degree-of-freedom tangential and normal skin deformation feedback," in *Proc. IEEE Haptics Symp. (HAPTICS)*, Feb. 2014, pp. 27–33.

[17] D. F. Collins, K. M. Refshauge, G. Todd, and S. C. Gandevia, "Cutaneous receptors contribute to kinesthesia at the index finger, elbow, and knee," *J. Neurophysiol.*, vol. 94, no. 3, pp. 1699–1706, Sep. 2005.

[18] S. Kanjanapas, C. M. Nunez, S. R. Williams, A. M. Okamura, and M. Luo, "Design and analysis of pneumatic 2-DoF soft haptic devices for shear display," *IEEE Robot. Autom. Lett.*, vol. 4, no. 2, pp. 1365–1371, Apr. 2019.

[19] S. B. Schorr, Z. F. Quek, R. Y. Romano, I. Nisky, W. R. Provancher, and A. M. Okamura, "Sensory substitution via cutaneous skin stretch feedback," in *Proc. IEEE Int. Conf. Robot. Autom.*, May 2013, pp. 2341–2346.

[20] H. Culbertson, S. B. Schorr, and A. M. Okamura, "Haptics: The present and future of artificial touch sensation," *Annu. Rev. Control, Robot., Auto. Syst.*, vol. 1, pp. 385–409, May 2018.

[21] C. Pacchierotti, A. Tirmizi, and D. Prattichizzo, "Improving transparency in teleoperation by means of cutaneous tactile force feedback," *ACM Trans. Appl. Perception*, vol. 11, no. 1, pp. 1–16, Apr. 2014.

[22] D. Leonardis, M. Solazzi, I. Bortone, and A. Frisoli, "A wearable fingertip haptic device with 3 DoF asymmetric 3-RSR kinematics," in *Proc. IEEE World Haptics Conf. (WHC)*, Jun. 2015, pp. 388–393.

[23] M. Solazzi, A. Frisoli, and M. Bergamasco, "Design of a novel finger haptic interface for contact and orientation display," in *Proc. IEEE Haptics Symp.*, Mar. 2010, pp. 129–132.

[24] S. B. Schorr and A. M. Okamura, "Three-dimensional skin deformation as force substitution: Wearable device design and performance during haptic exploration of virtual environments," *IEEE Trans. Haptics*, vol. 10, no. 3, pp. 418–430, Jul. 2017.

[25] B. Gleeson, S. Horschel, and W. Provancher, "Design of a fingertip-mounted tactile display with tangential skin displacement feedback," *IEEE Trans. Haptics*, vol. 3, no. 4, pp. 297–301, Oct. 2010.

[26] K. Minamizawa, H. Kajimoto, N. Kawakami, and S. Tachi, "A wearable haptic display to present the gravity sensation–preliminary observations and device design," in *Proc. 2nd Joint EuroHaptics Conf. Symp. Haptic Interfaces Virtual Environ. Teleoperator Syst. (WHC)*, Mar. 2007, pp. 133–138.

[27] J.-B. Chossat, D. K. Y. Chen, Y.-L. Park, and P. B. Shull, "Soft wearable skin-stretch device for haptic feedback using twisted and coiled polymer actuators," *IEEE Trans. Haptics*, vol. 12, no. 4, pp. 521–532, Oct. 2019.

[28] K. T. Yoshida, C. M. Nunez, S. R. Williams, A. M. Okamura, and M. Luo, "3-DoF wearable, pneumatic haptic device to deliver normal, shear, vibration, and torsion feedback," in *Proc. IEEE World Haptics Conf. (WHC)*, Jul. 2019, pp. 97–102.

[29] T. N. Do, H. Phan, T.-Q. Nguyen, and Y. Visell, "Miniature soft electromagnetic actuators for robotic applications," *Adv. Funct. Mater.*, vol. 28, no. 18, May 2018, Art. no. 1800244.

[30] T. N. Do, H. Phan, T.-Q. Nguyen, and Y. Visell, "Soft electromagnetic actuators: Miniature soft electromagnetic actuators for robotic applications (Adv. Funct. Mater. 18/2018)," *Adv. Funct. Mater.*, vol. 28, no. 18, May 2018, Art. no. 1870116.

[31] T. N. Do and Y. Visell, "Stretchable, twisted conductive microtubules for wearable computing, robotics, electronics, and healthcare," *Sci. Rep.*, vol. 7, no. 1, pp. 1–12, Dec. 2017.

[32] T. Kanno, S. Ohkura, O. Azami, T. Miyazaki, T. Kawase, and K. Kawashima, "Model of a coil-reinforced cylindrical soft actuator," *Appl. Sci.*, vol. 9, no. 10, p. 2109, May 2019.

[33] M. Zhu, T. N. Do, E. Hawkes, and Y. Visell, "Fluidic fabric muscle sheets for wearable and soft robotics," *Soft Robot.*, vol. 7, no. 2, pp. 179–197, Apr. 2020.

[34] M.-T. Thai and J.-R. Lee, "Hierarchical non-destructive testing scheme using laser ultrasonic propagation imager with broadband excitation and band divider," in *Proc. 9th NUAA-KAIST Joint Symp. Aerosp. Eng.*, Nanjing University of Aeronautics and Astronautics, no. 9, 2018, p. 27.

[35] M.-T. Thai, H. Ahmed, S.-C. Hong, J.-R. Lee, and J.-B. Ihn, "Broadband laser ultrasonic excitation and multi-band sensing for hierarchical automatic damage visualization," *Int. J. Aeronaut. Space Sci.*, vol. 20, no. 4, pp. 913–932, Dec. 2019.

[36] T. N. Do, T. Tjahjowidodo, M. W. S. Lau, and S. J. Phee, "Position control of asymmetric nonlinearities for a cable-conduit mechanism," *IEEE Trans. Autom. Sci. Eng.*, vol. 14, no. 3, pp. 1515–1523, Jul. 2017.

[37] T. N. Do, T. Tjahjowidodo, M. W. S. Lau, and S. J. Phee, "Adaptive control for enhancing tracking performances of flexible tendon–sheath mechanism in natural orifice transluminal endoscopic surgery (NOTES)," *Mechatronics*, vol. 28, pp. 67–78, Jun. 2015.

[38] M. Paré, H. Carnahan, and A. Smith, "Magnitude estimation of tangential force applied to the fingerpad," *Exp. Brain Res.*, vol. 142, no. 3, pp. 342–348, Feb. 2002.

[39] B. B. Edin, "Quantitative analyses of dynamic strain sensitivity in human skin mechanoreceptors," *J. Neurophysiol.*, vol. 92, no. 6, pp. 3233–3243, Dec. 2004.

[40] H. M. Le, T. N. Do, and S. J. Phee, "A survey on actuators-driven surgical robots," *Sens. Actuators A, Phys.*, vol. 247, pp. 323–354, Aug. 2016.

[41] M. T. Thai, P. T. Phan, T. T. Hoang, S. Wong, N. H. Lovell, and T. N. Do, "Advanced intelligent systems for surgical robotics," *Adv. Intell. Syst.*, vol. 2, no. 8, Jun. 2020, Art. no. 1900138.

[42] Y.-T. Pan, H. U. Yoon, and P. Hur, "A portable sensory augmentation device for balance rehabilitation using fingertip skin stretch feedback," *IEEE Trans. Neural Syst. Rehabil. Eng.*, vol. 25, no. 1, pp. 31–39, Jan. 2017.

[43] G. Gerboni, A. Diodato, G. Ciuti, M. Cianchetti, and A. Menciassi, "Feedback control of soft robot actuators via commercial flex bend sensors," *IEEE/ASME Trans. Mechatronics*, vol. 22, no. 4, pp. 1881–1888, Aug. 2017.

[44] F. Chinello, C. Pacchierotti, J. Bimbo, N. G. Tsagarakis, and D. Prattichizzo, "Design and evaluation of a wearable skin stretch device for haptic guidance," *IEEE Robot. Autom. Lett.*, vol. 3, no. 1, pp. 524–531, Jan. 2018.

[45] B. T. Gleeson, S. K. Horschel, and W. R. Provancher, "Perception of direction for applied tangential skin displacement: Effects of speed, displacement, and repetition," *IEEE Trans. Haptics*, vol. 3, no. 3, pp. 177–188, Jul. 2010.

[46] T. N. Do, T. Tjahjowidodo, M. W. S. Lau, T. Yamamoto, and S. J. Phee, "Hysteresis modeling and position control of tendon-sheath mechanism in flexible endoscopic systems," *Mechatronics*, vol. 24, no. 1, pp. 12–22, Feb. 2014.

[47] T. N. Do, T. Tjahjowidodo, M. W. S. Lau, and S. J. Phee, "Real-time enhancement of tracking performances for cable-conduit mechanisms-driven flexible robots," *Robot. Comput.-Integr. Manuf.*, vol. 37, pp. 197–207, Feb. 2016.

[48] T. N. Do, T. E. T. Seah, and S. J. Phee, "Design and control of a mechatronic tracheostomy tube for automated tracheal suctioning," *IEEE Trans. Biomed. Eng.*, vol. 63, no. 6, pp. 1229–1238, Jun. 2016.

[49] T. L. Nguyen, T. N. Do, M. W. S. Lau, and S. J. Phee, "Modelling, design, and control of a robotic running foot for footwear testing with flexible actuator," presented at the 1st Int. Conf. Sports Sci. Technol. (ICSST), Singapore, 2014, pp. 505–514.

PHUOC THIEN PHAN received the B.Eng. degree in mechanical engineering from Vietnam National University, Ho Chi Minh City University of Technology (HCMUT), in 2015. He is currently pursuing the Ph.D. degree with the Graduate School of Biomedical Engineering, University of New South Wales (UNSW), Sydney, NSW, Australia. From 2016 to 2019, he was a Research Assistant with the School of Mechanical and Aerospace Engineering, Nanyang Technological University (NTU), Singapore. He developed a novel magnetically actuated soft capsule for obesity treatment and also involved several projects to flexible endoscopic systems. His research interests include flexible surgical devices, medical robotics, soft robotics, and capsule endoscopy.

NIGEL HAMILTON LOVELL (Fellow, IEEE) received the B.E. (Hons.) and Ph.D. degrees from the University of New South Wales (UNSW), Sydney, NSW, Australia. He is currently the Head of the Graduate School of Biomedical Engineering, UNSW, where he is also a Scientia Professor and the Head of the School. Through a spin-out company from UNSW, TeleMedCare Pty. Ltd. that he co-founded, he has commercialised a range of tele-health technologies for managing chronic disease and falls in the older population. He is also one of the key researchers leading a research and development program to develop in Australia a retinal neuroprosthesis or bionic eye. He has authored more than 250 journal articles and been awarded over $80 million in research and development and infrastructure funding. He has mentored 70 Ph.D. students and delivered more than a hundred keynote presentations. His research interests include cardiac and retinal modeling, medical informatics and data analytics especially related to telehealth technologies, biological signal processing, and visual prosthesis design. He is a Fellow of seven learned academies throughout the world, including AIMBE. From 2017 to 2018, he was the President of the World's Largest Biomedical Engineering Society – the IEEE Engineering in Medicine and Biology Society.

MAI THANH THAI received the B.Eng. degree in mechatronic engineering from the Ho Chi Minh City University of Technology (HCMUT), Vietnam, in 2016, and the M.S. degree in aerospace engineering from the Korea Advanced Institute of Science and Technology (KAIST), South Korea, in 2019. He is currently pursuing the Ph.D. degree with the Graduate School of Biomedical Engineering, University of New South Wales (UNSW), Sydney, NSW, Australia. His research interests include wearable haptic devices, medical robotics, flexible surgical devices, soft robotics, soft actuators, and advanced control algorithms.

TRUNG THIEN HOANG received the B.Eng. degree in biomedical engineering from International University, Vietnam National University, Ho Chi Minh City, Vietnam. He is currently pursuing the Ph.D. degree with the Graduate School of Biomedical Engineering, University of New South Wales (UNSW), Sydney, NSW, Australia. His research interests include wearable and miniaturized medical devices, biosensors, point–of–care diagnostic devices/solutions, medical robotics, functional materials, and soft robotics.

THANH NHO DO (Member, IEEE) received the Ph.D. degree in surgical robotics from the School of Mechanical and Aerospace Engineering (MAE), Nanyang Technological University (NTU), Singapore, in 2015. He was a Postdoctoral Scholar with the California NanoSystems Institute, University of California Santa Barbara, USA. He also worked as a Research Fellow with the Robotic Research Center, School of MAE, NTU. He is currently a Scientia Lecturer with the Graduate School of Biomedical Engineering, University of New South Wales (UNSW), Sydney, NSW, Australia. He directs the UNSW Medical Robotics Laboratory. His research interests include soft robotics, wearable haptics, control, surgical robotics, and mechatronics in medicine.

• • •